






Superconductivity in orthorhombic NbS

Bin-Bin Ruan ^{1,*}, Jun-Kun Yi ^{1,2,*}, Le-Wei Chen,^{1,2} Menghu Zhou ¹, Yun-Qing Shi,^{1,2} Qing-Song Yang ^{1,2},
Ya-Dong Gu,^{1,2} Gen-Fu Chen,^{1,2} and Zhi-An Ren ^{1,2,‡}

¹*Institute of Physics and Beijing National Laboratory for Condensed Matter Physics, Chinese Academy of Sciences, Beijing 100190, China*

²*School of Physical Sciences, University of Chinese Academy of Sciences, Beijing 100049, China*



(Received 18 August 2023; revised 13 October 2023; accepted 15 November 2023; published 27 November 2023)

Compared to the intensively studied niobium dichalcogenides, the physical properties of niobium monosulfide (NbS) have been less explored. Here we report the discovery of bulk superconductivity in orthorhombic NbS (*o*-NbS). First-principles results of *o*-NbS are also revealed. *o*-NbS crystallizes in a MnP-type structure (*Pnma*) with lattice parameters $a = 6.4450(1)$ Å, $b = 3.31770(4)$ Å, and $c = 5.8629(1)$ Å. It exhibits type-II superconductivity with a critical temperature (T_c) of 6.0 K. Bulk superconductivity is confirmed by the magnetization and heat capacity measurements. The upper and lower critical fields are 7.4 T and 13.0 mT, respectively. Specific heat data suggest that *o*-NbS is a fully gapped *s*-wave superconductor, with $\Delta_0/k_B T_c = 1.75$ and $\Delta C_e/\gamma T_c = 1.45$, fitting perfectly within the BCS theory. First-principles calculations indicate that the Nb-4*d* states dominate the Fermi level (E_F), and the density of states (DOS) on E_F is sensitive to niobium vacancies. Different from the quasi-two-dimensional $2H$ -NbS₂ and quasi-one-dimensional Nb₃S₄ superconductors, our discovery of superconductivity in three-dimensional *o*-NbS provides a different motif for both experimental and theoretical studies.

DOI: [10.1103/PhysRevB.108.174517](https://doi.org/10.1103/PhysRevB.108.174517)

I. INTRODUCTION

Transition-metal dichalcogenides (TMDs) have garnered much attention in recent years. Most of the TMDs consist of weakly bounded van der Waals layers, which not only give rise to charge density waves (CDWs) [1–3] but also enable delicate fabrication of electronic devices [4,5]. When it comes to superconductivity, the group-5 TMDs, basically TCh_2 ($T = \text{Nb, Ta}$, $Ch = \text{S, Se}$), are the primary focus. Intriguing phenomena, including electron-phonon-driven CDWs [6–8], Ising pairing [9,10], orbital-selective multigap superconductivity [11,12], and topological surface states [13], have been observed in $2H$ -Nb(S₂, Se₂). These findings have also inspired researchers to explore new superconductors in the Nb-S and Nb-Se systems. In addition to $2H$ -NbS₂, which exhibits a transition temperature (T_c) of 6.2 K [14,15], superconductivity has also been identified in intercalated NbS₂ [16] and in Nb₂₁S₈ [17].

Unlike the other members in the Nb-S phase diagram, niobium monosulfide (NbS) has rarely been studied. The existence of NbS has been known since 1938 [18], yet its crystal structure remained elusive until Schönberg reported a hexagonal lattice in 1954 [19]. In 1969, another orthorhombic polymorph of NbS was discovered [20]. Hexagonal NbS (*h*-NbS) was found to undergo a reversible phase transition to the high-temperature orthorhombic form (*o*-NbS) at 1053 K [20]. Despite *o*-NbS been known for over 50 years, its physical properties remain largely unexplored. To the best

of our knowledge, there are only two references mentioning the transport property of NbS [21,22]. In 1954, Hardy and Hulm performed magnetic measurements on a NbS sample (structure not disclosed), in which no superconductivity was detected above 1.28 K [21]. On the contrary, Narayan and Finnemore reported 3.8 K superconductivity in “orthorhombic NbS” [22]. However, the lattice parameters in Ref. [22] significantly deviated (by 17%) from previous reports on *o*-NbS single crystals [20], casting doubt on the reliability. Furthermore, no information about the phase purity or evidence of bulk superconductivity was provided. Note that there are other superconducting Nb-S phases, including $2H$ -NbS₂ ($T_c = 6.2$ K) [14], Nb₃S₄ ($T_c = 4.0$ K) [23], and Nb₂₁S₈ ($T_c = 4.1$ K) [17]. Therefore, one should be very careful to rule out potential contamination from these impurities.

From a theoretical point of view, *o*-NbS would be an interesting motif to study, should the superconductivity be confirmed. First, different from its low-dimensional relatives (NbS₂, NbS₃, or Nb₃S₄) [23–25], *o*-NbS hosts a unique three-dimensional crystal structure. Second, NbS is arguably the simplest compound in the Nb-S system, making it a favorable candidate for theoretical research. Unexpectedly, no first-principles studies have been reported for such a simple compound. Lucrezi and Heil explored the binary Nb-S system with *ab initio* predictions, but they somehow omitted *o*-NbS [26]. Very recently, An *et al.* performed density functional theory (DFT) calculations on *h*-NbS without mentioning *o*-NbS [27]. Checking major material databases such as the Materials Project [28], Materialia [29], or Atomly [30], one can find over 100 entries of first-principles results for binary Nb-S compounds. However, none of these databases includes information about *o*-NbS. To date, basic knowledge such as the electronic band structure of *o*-NbS is still lacking.

*These authors contributed equally to this work.

†bbuan@mail.ustc.edu.cn

‡renzhian@iphy.ac.cn

In this study, we report the observation of bulk superconductivity at 6.0 K in *o*-NbS. Superconducting properties are investigated in detail employing electrical, magnetic, and heat transport measurements. Subsequently, the superconducting parameters for *o*-NbS are determined. In addition, first-principles calculations reveal the dominant role of the Nb-4*d* states.

II. METHODS

Polycrystalline samples of *o*-NbS were synthesized by solid-state reactions. The starting materials were Nb (powder, Aladdin Reagents, 99.95%) and S (powder, Alfa Aesar, 99.999%). To prevent the formation of Nb₃S₄ and minimize niobium vacancies, Nb and S were mixed in a molar ratio of 1.05:1. The mixture was pressed into pellets, placed in evacuated quartz tubes, and annealed at 1363 K for 20 hours before cooled down to 1173 K. The quartz tubes were subsequently quenched in ice water to preserve the orthorhombic NbS phase. The products were ground into fine powder, pressed into pellets, and subjected to one more annealing cycle under the same condition. The final products were black and appeared to be stable under ambient conditions. However, given reports of the degradation of 2*H*-NbS₂ in air [31], *o*-NbS was kept in high-purity argon before use.

A powder x-ray diffraction (XRD) pattern at room temperature was collected with a PAN-analytical x-ray diffractometer (Cu-*K*α radiation). The Rietveld refinement of XRD was performed with the GSAS package [32]. Electrical resistivity was measured on a rectangular cut, using a Quantum Design physical property measurement system (PPMS). The standard four-probe technique was applied. The heat capacity was also measured on a PPMS, using the relaxation method. The magnetic properties were measured on a Quantum Design magnetic property measurement system (MPMS). Note that the magnetic fields in this study have been corrected considering the demagnetization factors [33].

DFT calculations were performed using the QUANTUM ESPRESSO (QE) package [34]. The generalized gradient approximation (GGA) and Perdew-Burke-Ernzerhof (PBE) exchange-correlation functionals were applied. The optimized norm-conserving pseudopotentials of Nb and S were chosen [35]. The energy cutoffs for the wave functions were 60 Ry. The crystal structure was fully relaxed until the force on each atom was less than 0.0002 Ry Bohr⁻¹. Monkhorst-Pack *k*-point grids of 5 × 11 × 5 and 9 × 19 × 9 were used to calculate the charge densities, and the density of states (DOS), respectively. The calculations were performed without considering the spin-orbit-coupling (SOC) effects because SOC was found to introduce little change to the results.

III. RESULTS AND DISCUSSIONS

Figure 1 shows the powder XRD pattern of our *o*-NbS sample. The pattern was refined based on the orthorhombic NbS structure (*Pnma*), as determined from single crystals by Kadijk and Jellinek [20]. No *h*-NbS phase was detected. The converged refinement parameters $R_p = 1.93\%$, $R_{wp} = 2.89\%$, and $\chi^2 = 3.2$. The refinement results are plotted in Fig. 1. According to the refinement, there is about 1.1 wt.%

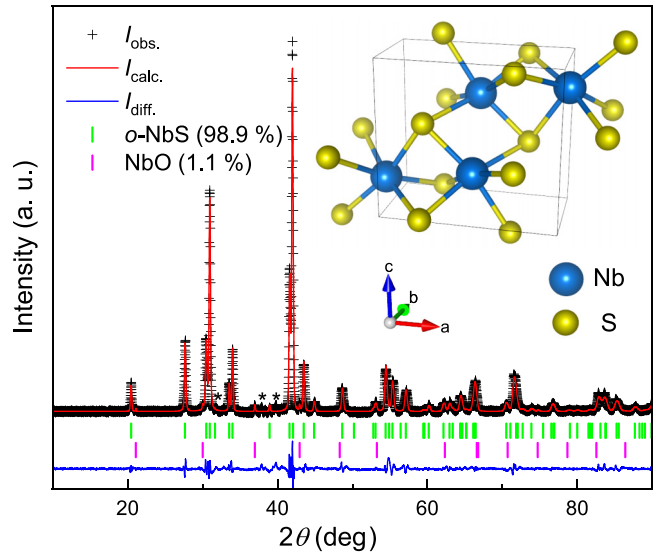


FIG. 1. Powder XRD pattern of NbS at room temperature. Solid lines show the Rietveld refinement results. Vertical bars indicate the Bragg positions from *o*-NbS and NbO. The asterisks denote peaks from an unidentified impurity. Inset: the crystal structure of *o*-NbS.

of NbO as the impurity. In addition, there is a tiny amount of unidentified impurity, which could be other, more complex niobium sulfides such as Nb₂₁S₈ [36] or Nb₁₄S₅ [37]. The refined cell parameters for *o*-NbS are $a = 6.4450(1)$ Å, $b = 3.31770(4)$ Å, and $c = 5.8629(1)$ Å. Further crystallographic details are provided in Table I.

The crystal structure of *o*-NbS is illustrated in the inset of Fig. 1. Both Nb and S atoms are in a distorted octahedral coordination environment, forming an orthorhombic MnP-type lattice. Different from layered NbS₂ or quasi-one-dimensional NbS₃ [24,25], *o*-NbS possesses a unique three-dimensional structure. According to previous reports [20], *o*-NbS can host niobium vacancies, resulting in compositions represented as Nb_{1-δ}S (0 ≤ δ ≤ 0.08). For δ = 0, the lattice parameters are $a = 6.446$ Å, $b = 3.326$ Å, and $c = 5.897$ Å, while for δ = 0.08, they are $a = 6.396$ Å, $b = 3.334$ Å, and $c = 5.845$ Å [20]. Our results of the lattice align with the δ = 0 case, implying that the niobium vacancies should be nearly zero. The full occupancy of Nb sites is also confirmed by the XRD refinement (Table I).

On the other hand, the DFT calculations give the relaxed lattice parameters as $a = 6.4619$ Å, $b = 3.3557$ Å, and $c = 6.0280$ Å. These values agree fairly well with the experimental ones, although the relaxed ones are slightly larger (which is common when using GGA functionals).

TABLE I. Crystallographic parameters of *o*-NbS from the Rietveld refinement of XRD. Space group *Pnma* (No. 62), $a = 6.4450(1)$ Å, $b = 3.31770(4)$ Å, $c = 5.8629(1)$ Å. U_{eq} is one-third of the trace of the U_{ij} tensor.

Atom (site)	<i>x</i>	<i>y</i>	<i>z</i>	U_{eq} (0.01Å ²)	Occupancy
Nb (4 <i>c</i>)	0.0061(3)	0.25	0.2140(1)	1.51(6)	1.0(0)
S (4 <i>c</i>)	0.2247(4)	0.25	0.5788(3)	0.47(7)	1.0(0)

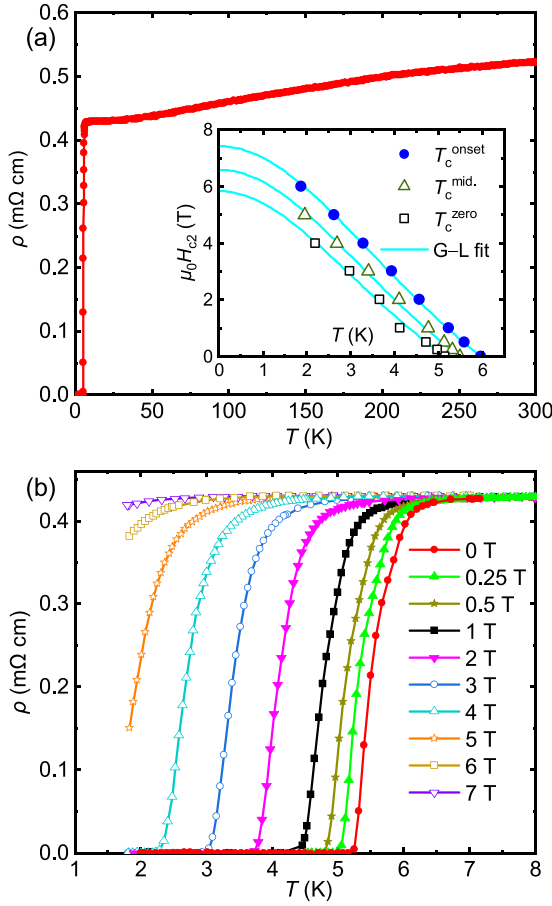


FIG. 2. (a) Temperature dependence of electronic resistivity of *o*-NbS under zero magnetic field. Inset: the T_c evolution with magnetic field; the solid lines are fits with the G-L model. (b) Superconducting transitions under different magnetic fields up to 7 T.

The temperature dependence of resistivity (ρ) of *o*-NbS is presented in Fig. 2(a). As the temperature decreases below 300 K, the resistivity of *o*-NbS decreases monotonically, demonstrating a metallic nature. The residual resistivity ratio [RRR = $\rho(300 \text{ K})/\rho(7 \text{ K}) = 1.24$] is rather small, suggesting the existence of atomic disorder. This may result from the intrinsic Nb vacancies in *o*-NbS, causing local off-stoichiometries. The low-temperature region of $\rho(T)$ is shown in Fig. 2(b), revealing a superconducting transition. We determine the onset value of the transition (T_c^{onset}), at which $\rho(T)$ reaches 90% of the resistance of the normal state; the midpoint of the transition ($T_c^{\text{mid.}}$), at which $\rho(T)$ reaches 50% of the normal state resistance; and T_c^{zero} , at which $\rho(T)$ drops to zero. T_c^{onset} , $T_c^{\text{mid.}}$, and T_c^{zero} are thus determined to be 6.0, 5.5, and 5.2 K, respectively.

The superconducting transition was suppressed as magnetic fields were applied, as depicted in Fig. 2(b). The evolution of T_c over the magnetic field is shown in the inset of Fig. 2(a). According to the Ginzburg-Landau (G-L) theory, the upper critical field [$\mu_0 H_{c2}(T)$] is fitted with $\mu_0 H_{c2}(T) = \mu_0 H_{c2}(0)(1 - t^2)/(1 + t^2)$, in which $t = T/T_c$ [38]. $\mu_0 H_{c2}(0)$ is determined to be 7.4 T from the T_c^{onset} curve. In contrast to $2H\text{-NbS}_2$ [39], *o*-NbS exhibits no evident signatures of multi-gap superconductivity [i.e., upward curvature in $\mu_0 H_{c2}(T)$].

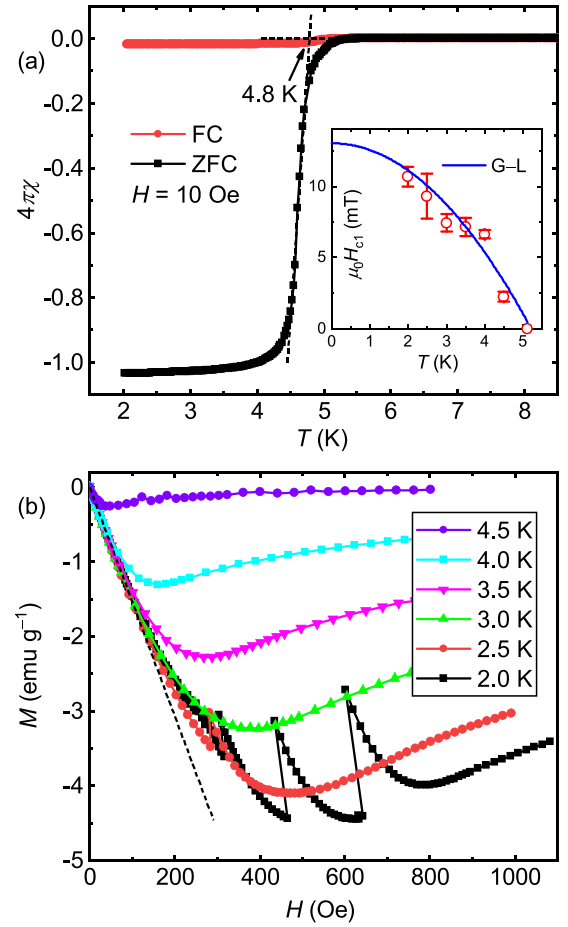


FIG. 3. (a) Temperature dependence of DC magnetic susceptibility of *o*-NbS. Inset: the temperature dependence of lower critical field $\mu_0 H_{c1}(T)$. The solid line is a fit with the G-L model. (b) Field-dependent magnetization of *o*-NbS at different temperatures below T_c . The discontinuous points are due to avalanches caused by flux jump. The dashed line guides the Meissner states.

The superconductivity of *o*-NbS was further confirmed by temperature-dependent magnetization measurements. The results are shown in Fig. 3. The demagnetization factor (N) for the rectangular sample (of dimensions $a \times b \times c$) was determined by $N = ab/[ab + 3c(a + b)]/4$ [33]. Both the zero-field-cooled (ZFC) and field-cooled (FC) DC magnetic susceptibility ($4\pi\chi$) curves exhibit a superconducting transition below 5.4 K, consistent with the $\rho(T)$ results. T_c determined from the intersection of normal state $4\pi\chi(T)$ and the steepest slope is 4.8 K. The ZFC $4\pi\chi$ approaches 100% at 2.0 K, confirming the existence of bulk superconductivity. Figure 3(b) demonstrates the isothermal magnetization [$M(H)$] curves at different temperatures. These curves exhibit behaviors of a typical type-II superconductor. One interesting feature is that the $M(H)$ curves at 2.0 and 2.5 K show discontinuities from flux jumps, which are explained by the adiabatic model [40]. According to this model, when dissipative heat generated by vortex movements is not promptly absorbed, a small thermal fluctuation can eventually trigger avalanche-like heating, which brings part of the superconductor to the normal state. Flux jumps have been frequently observed in Nb-based

TABLE II. Superconducting and thermodynamic parameters of *o*-NbS.

Parameter	Unit	Value
T_c^{onset}	K	6.0
T_c^{zero}	K	5.2
$\mu_0 H_{c1}(0)$	mT	13.0
$\mu_0 H_{c2}(0)^a$	T	7.4
ξ_{GL}	nm	7.5
λ_{GL}	nm	221.0
κ_{GL}		29.4
γ	$\text{mJ mol}^{-1} \text{K}^{-2}$	4.87
β	$\text{mJ mol}^{-1} \text{K}^{-4}$	0.060
Θ_{D}	K	402
λ_{ep}		0.59
$\Delta C_e / \gamma T_c$		1.45
Δ_0	meV	0.77
$N(E_{\text{F}})$	$\text{eV}^{-1} \text{f.u.}^{-1}$	1.30

^aFrom T_c^{onset} .

alloy superconductors [41], MgB_2 [42], and iron-based superconductors [43]. Nevertheless, we can still get the lower critical fields ($\mu_0 H_{c1}$) from the deviations of $M(H)$ from the initial Meissner states. The temperature dependence of $\mu_0 H_{c1}$ is summarized in the inset of Fig. 3(a). $\mu_0 H_{c1}(T)$ is fitted with the G-L formula [38]: $\mu_0 H_{c1}(T) = \mu_0 H_{c1}(0)[1 - (T/T_c)^2]$ (shown as the solid line), yielding an estimated value of $\mu_0 H_{c1}(0)$ to be 13.0 mT.

Gathering results from the resistivity and magnetization measurements, we are able to estimate the basic superconducting parameters of *o*-NbS. The coherence length (ξ_{GL}) is determined by [38]

$$\mu_0 H_{c2}(0) = \Phi_0 / (2\pi \xi_{\text{GL}}^2), \quad (1)$$

in which Φ_0 is the flux quantum. Note that $\mu_0 H_{c2}(0)$ in Eq. (1) represents the one determined from T_c^{zero} . The penetration depth (λ_{GL}) is calculated by [44]

$$\mu_0 H_{c1}(0) = \frac{\Phi_0}{4\pi \lambda_{\text{GL}}^2} [\ln(\kappa_{\text{GL}}) + 0.5], \quad (2)$$

in which $\kappa_{\text{GL}} \equiv \lambda_{\text{GL}} / \xi_{\text{GL}}$ is the G-L parameter. From Eqs. (1) and (2), ξ_{GL} , λ_{GL} , and κ_{GL} are estimated to be 7.5 and 221.0 nm, and 29.4, respectively. Note that κ_{GL} is obviously larger than $1/\sqrt{2}$, suggesting type-II superconductivity in *o*-NbS. In addition, we estimate the thermodynamic field [$\mu_0 H_c(0)$] to be 0.15 T by $H_c^2(0) \ln \kappa_{\text{GL}} = H_{c1}(0) H_{c2}(0)$. These superconducting parameters are summarized in Table II.

To gain further insight into the superconductivity, we conducted specific heat (C_p) measurements on *o*-NbS, and the results are shown in Fig. 4(a). The $C_p(T)$ curve under zero magnetic field records a pronounced peak below 6.0 K, confirming the bulk superconductivity. Under a field of 8 T, the superconducting transition is completely suppressed. The curve at 8 T is well fitted with the standard Debye model $C_p(T)/T = \gamma + \beta T^2$, with $\gamma = 4.87 \text{ mJ mol}^{-1} \text{K}^{-2}$ and $\beta = 0.060 \text{ mJ mol}^{-1} \text{K}^{-4}$. Consequently, the Debye temperature (Θ_{D}) is estimated to be 402 K by $\Theta_{\text{D}} = (12\pi^4 NR/5\beta)^{1/3}$, in which R is the ideal gas constant and $N = 2$.

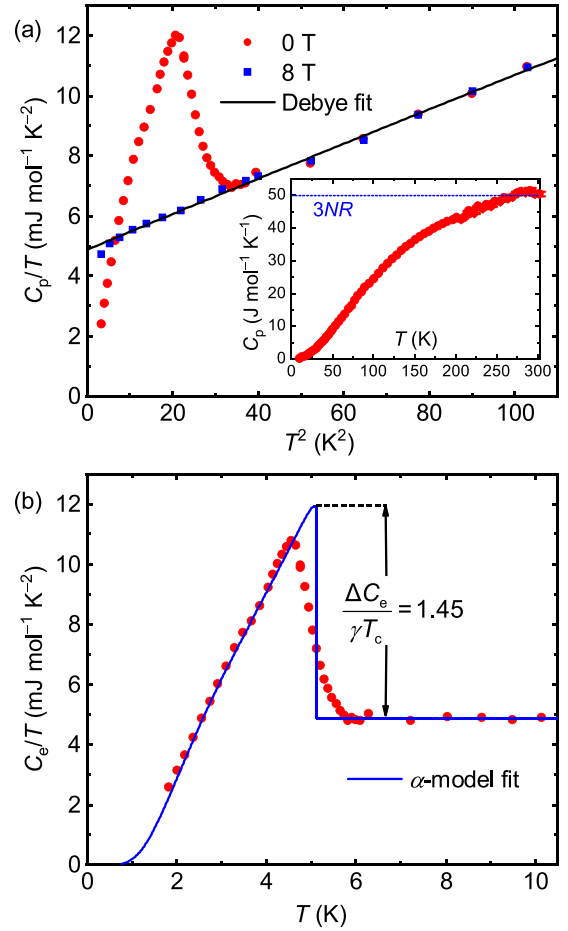


FIG. 4. (a) Temperature-dependent specific heat (C_p) of *o*-NbS under zero and 8 T magnetic field. The solid line is a fit with the Debye model. Inset: $C_p(T)$ from 10 to 300 K. (b) Temperature-dependent electronic specific heat (C_e) under zero magnetic field. The solid lines are a fit with the α model.

The $C_p(T)$ data from 10 to 300 K under zero magnetic field are presented in the inset of Fig. 4(a). By combining the results from the resistivity [Fig. 2(a)] and specific heat measurements, we conclude that there are no structural phase transitions or CDW orders occurring below 300 K.

We further obtained the electronic specific heat (C_e) by subtracting the phononic terms [Fig. 4(b)]. T_c estimated from $C_e(T)$ is 5.1 K, which reasonably agrees with the values from the resistivity and magnetization measurements. $C_e(T)$ in the superconducting state is fitted with the α model [45], in which the entropy

$$S(T) = -\frac{6\gamma}{\pi^2 k_{\text{B}}} \int_0^\infty [f \ln f + (1-f) \ln(1-f)] d\epsilon, \quad (3)$$

$f = 1 / \{1 + \exp[\sqrt{\epsilon^2 + \Delta^2(T)} / k_{\text{B}} T]\}$, and the isotropic gap function $\Delta(T) = \Delta_0 \tanh\{1.82[1.018(T_c/T - 1)]^{0.51}\}$ (k_{B} is the Boltzmann constant). As shown in Fig. 4(b), the experimental data are well described by the α model, implying *o*-NbS possibly to be an *s*-wave superconductor. Additionally, the zero-temperature superconducting gap (Δ_0) is fitted to be 0.77 meV. Both the coupling strength ($\Delta_0/k_{\text{B}} T_c = 1.75$) and the normalized C_e jump ($\Delta C_e / \gamma T_c = 1.45$) perfectly agree

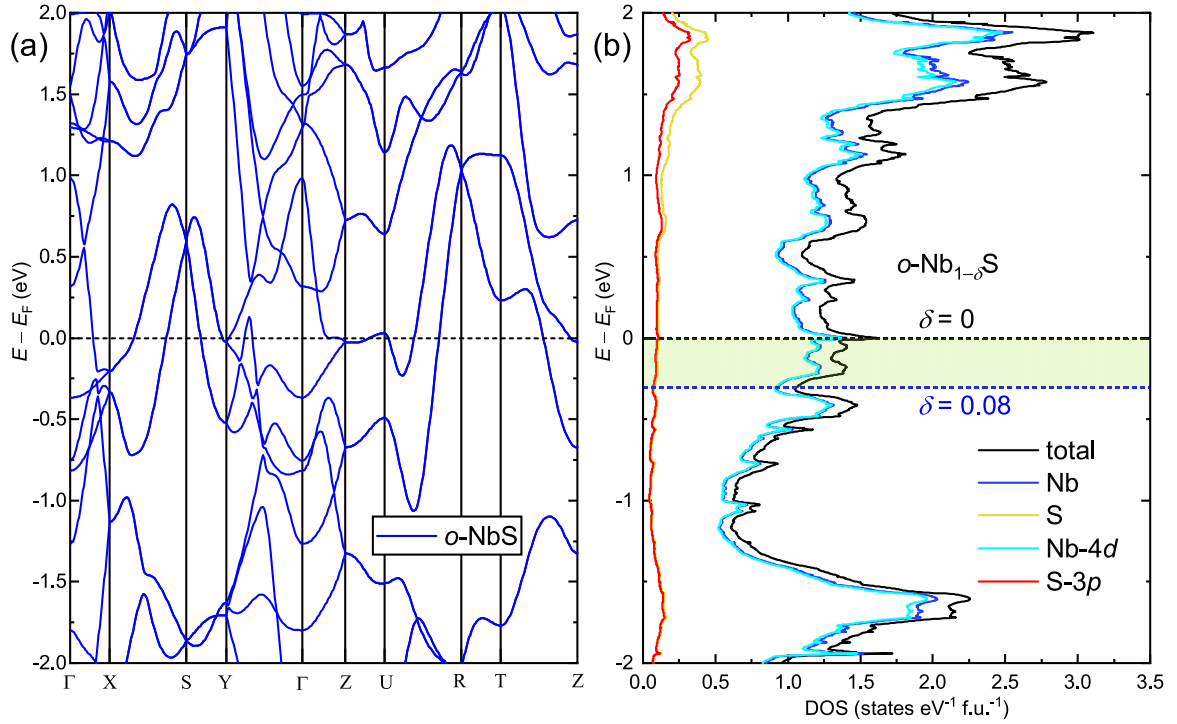


FIG. 5. (a) DFT electronic band structure of o -NbS without SOC near the Fermi level (E_F). (b) Calculated DOS of o -NbS near E_F . The E_F window for o -Nb $_{1-\delta}$ S ($0 \leq \delta \leq 0.08$) is also plotted.

with the Bardeen-Cooper-Schrieffer (BCS) weak-coupling ratios (1.76 and 1.43, respectively) [46].

The electron-phonon coupling constant λ_{ep} is estimated by the McMillan relation [47],

$$\lambda_{ep} = \frac{1.04 + \mu^* \ln(\Theta_D/1.45T_c)}{(1 - 0.62\mu^*) \ln(\Theta_D/1.45T_c) - 1.04}, \quad (4)$$

where μ^* is the Coulomb pseudopotential parameter. For $\mu^* = 0.13$, $\lambda_{ep} = 0.59$ is obtained, again suggesting weak electron-phonon coupling. Based on the values of γ and λ_{ep} , the DOS at the Fermi level $N(E_F) = 3\gamma/[\pi^2 k_B^2 (1 + \lambda_{ep})] = 1.30$ states eV^{-1} per formula unit (f.u.).

Figure 5 summarizes the calculated electronic band structures and DOS near the Fermi level (E_F). The k -path labels are from the SEEK-PATH code [48]. Multiple bands cross E_F , confirming the metallic nature of o -NbS. Most of the bands show relatively large energy dispersion, implying that the correlation effects might be insignificant. As shown in Fig. 5(b), the states near E_F are dominated by the Nb electrons, with minor contributions from S. Most of the Nb states originate from Nb-4d orbitals, while the S states are mainly from S-3p. Note that E_F of stoichiometric o -NbS locates at a sharp peak on the DOS curve. And the DOS value reads 1.59 states eV^{-1} f.u. $^{-1}$ at E_F . At first glance, this value differs from the experimental $N(E_F)$ (1.30 states eV^{-1} f.u. $^{-1}$). However, when considering the Nb vacancies, DOS at E_F is expected to be lower. Figure 5(b) shows the window of E_F of o -Nb $_{1-\delta}$ S ($0 \leq \delta \leq 0.08$) assuming a rigid band. DOS on E_F will drastically reduce to 1.35 states eV^{-1} f.u. $^{-1}$ even when $\delta = 0.005$.

Such sensitivity of $N(E_F)$ to small changes in niobium vacancies may explain the conflicting results of NbS

properties in previous studies. According to McMillan's formalism [47], λ_{ep} is expressed as $[N(E_F)\langle I^2 \rangle]/[M\langle \omega^2 \rangle]$, in which M is the atomic mass, and $\langle I^2 \rangle$ and $\langle \omega^2 \rangle$ stand for average electron-phonon matrix elements, and phonon frequencies, respectively. As δ in o -Nb $_{1-\delta}$ S increases from 0 to 0.08, $N(E_F)$ is reduced from 1.59 to 1.05 states eV^{-1} f.u. $^{-1}$ [Fig. 5(b)]. Consequently, T_c will be lowered too. The existence of Nb vacancies leads to an enhancement of defect scattering, which is also damaging to superconductivity. As a result, superconductivity fades with increasing δ . This could be the reason why Hardy *et al.* failed to observe superconductivity above 1.28 K [21], and why Narayan *et al.* reported a much lower T_c (3.8 K) [22]. Neither of the previous studies on NbS provided sufficient information regarding the lattice parameters, so it is hard to estimate the Nb vacancies in their samples. Nevertheless, Narayan *et al.* did notice that T_c "appears to drop with increasing sulfur content" [22], consistent with the above analysis.

Superconductivity in other niobium-based TMDs is similarly sensitive to stoichiometry. For instance, in $2H$ -Nb $_{1+\delta}$ Se $_2$, T_c sharply drops from 7.2 to 2.2 K as δ increases from 0 to 0.05 [49]. In $2H$ -NbS $_{2-y}$, T_c drops from 6.2 to 2.2 K as y changes from 0 to 0.1 [50]. These studies, together with our present results, emphasize the importance of atomic stoichiometry in the exploration of new niobium-based superconducting materials.

IV. CONCLUSIONS

In conclusion, we have reported the discovery and detailed investigation of bulk superconductivity in o -NbS. o -NbS turns out to be a type-II superconductor with $T_c = 6.0$ K, and upper and lower critical fields to be 7.4 T and 13.0 mT,

respectively. The coupling strength ($\Delta_0/k_B T_c = 1.75$) and normalized C_c change ($\Delta C_c/\gamma T_c = 1.45$) closely match the BCS theory, evidencing weak electron-phonon coupling. We have also reported the DFT results of *o*-NbS, from which E_F of stoichiometric *o*-NbS is found to locate at a sharp peak on the DOS curve. Different from layered *2H*-Nb(S,Se)₂ superconductors, *o*-NbS features a unique three-dimensional MnP-type crystal structure, thus offering a different platform to study the interplay between dimensionality, stoichiometries, and superconductivity in niobium chalcogenide superconductors.

ACKNOWLEDGMENTS

The crystal structure was illustrated by the VESTA software [51]. This work was supported by the National Key Research and Development Program of China (Grants No. 2018YFA0704200 and No. 2021YFA1401800), the National Natural Science Foundation of China (Grant No. 12074414), and the Strategic Priority Research Program of Chinese Academy of Sciences (Grant No. XDB25000000).

The authors declare that they have no conflict of interest.

-
- [1] K. Cho, M. Kończykowski, S. Teknowijoyo, M. A. Tanatar, J. Guss, P. Gartin, J. Wilde, A. Kreyssig, R. McQueeney, A. I. Goldman *et al.*, Using controlled disorder to probe the interplay between charge order and superconductivity in NbSe₂, *Nat. Commun.* **9**, 2796 (2018).
- [2] S. Ni, M. Zhou, Z. Lin, B. Ruan, Z. Li, Z. Zou, Z. Xu, and Z.-A. Ren, Crystal growth, superconductivity, and charge density wave of pristine and Pd-intercalated *2H*-TaS₂, *Phys. Rev. B* **108**, 075103 (2023).
- [3] B. Sipoš, A. F. Kusmartseva, A. Akrap, H. Berger, L. Forró, and E. Tutiš, From Mott state to superconductivity in 1T-TaS₂, *Nat. Mater.* **7**, 960 (2008).
- [4] D. K. Efetov, L. Wang, C. Handschin, K. Efetov, J. Shuang, R. Cava, T. Taniguchi, K. Watanabe, J. Hone, C. Dean *et al.*, Specular interband Andreev reflections at van der Waals interfaces between graphene and NbSe₂, *Nat. Phys.* **12**, 328 (2016).
- [5] N. Yabuki, R. Moriya, M. Arai, Y. Sata, S. Morikawa, S. Masubuchi, and T. Machida, Supercurrent in van der Waals Josephson junction. *Nat. Commun.* **7**, 10616 (2016).
- [6] T. Valla, A. V. Fedorov, P. D. Johnson, P. A. Glans, C. McGuinness, K. E. Smith, E. Y. Andrei, and H. Berger, Quasi-particle spectra, charge-density waves, superconductivity, and electron-phonon coupling in *2H*-NbSe₂, *Phys. Rev. Lett.* **92**, 086401 (2004).
- [7] F. Weber, S. Rosenkranz, J.-P. Castellan, R. Osborn, R. Hott, R. Heid, K.-P. Bohnen, T. Egami, A. H. Said, and D. Reznik, Extended phonon collapse and the origin of the charge-density wave in *2H*-NbSe₂, *Phys. Rev. Lett.* **107**, 107403 (2011).
- [8] C. D. Malliakas and M. G. Kanatzidis, Nb–Nb interactions define the charge density wave structure of *2H*-NbSe₂, *J. Am. Chem. Soc.* **135**, 1719 (2013).
- [9] X. Xi, Z. Wang, W. Zhao, J.-H. Park, K. T. Law, H. Berger, L. Forró, J. Shan, and K. F. Mak, Ising pairing in superconducting NbSe₂ atomic layers, *Nat. Phys.* **12**, 139 (2016).
- [10] H. Zhang, A. Rousuli, K. Zhang, L. Luo, C. Guo, X. Cong, Z. Lin, C. Bao, H. Zhang, S. Xu *et al.*, Tailored ising superconductivity in intercalated bulk NbSe₂, *Nat. Phys.* **18**, 1425 (2022).
- [11] T. Yokoya, T. Kiss, A. Chainani, S. Shin, M. Nohara, and H. Takagi, Fermi surface sheet-dependent superconductivity in *2H*-NbSe₂, *Science* **294**, 2518 (2001).
- [12] X. Bi, Z. Li, J. Huang, F. Qin, C. Zhang, Z. Xu, L. Zhou, M. Tang, C. Qiu, P. Tang *et al.*, Orbital-selective two-dimensional superconductivity in *2H*-NbSe₂, *Phys. Rev. Res.* **4**, 013188 (2022).
- [13] J.-P. Xu, M.-X. Wang, Z. L. Liu, J.-F. Ge, X. Yang, C. Liu, Z. A. Xu, D. Guan, C. L. Gao, D. Qian *et al.*, Experimental detection of a majorana mode in the core of a magnetic vortex inside a topological insulator-superconductor Bi₂Te₃/NbSe₂ heterostructure, *Phys. Rev. Lett.* **114**, 017001 (2015).
- [14] M. Van Maaren and G. Schaeffer, Superconductivity in group V^a dichalcogenides, *Phys. Lett.* **20**, 131 (1966).
- [15] C. Witteveen, K. Górnicka, J. Chang, M. Månsson, T. Klimczuk, and F. O. von Rohr, Polytypism and superconductivity in the NbS₂ system, *Dalton Trans.* **50**, 3216 (2021).
- [16] A. Devarakonda, H. Inoue, S. Fang, C. Ozsoy-Keskinbora, T. Suzuki, M. Kriener, L. Fu, E. Kaxiras, D. C. Bell, and J. G. Checkelsky, Clean 2D superconductivity in a bulk van der Waals superlattice, *Science* **370**, 231 (2020).
- [17] M. Köckerling, D. Johrendt, and E. W. Finckh, Superconductivity in Nb₂₁S₈, a phase with metal cluster chains, *J. Am. Chem. Soc.* **120**, 12297 (1998).
- [18] W. Blitz and A. Köcher, On the niobium/sulfur system, *Z. Anorg. Allg. Chem.* **237**, 369 (1938).
- [19] N. Schönberg, The tungsten carbide and nickel arsenide structures, *Acta Metall.* **2**, 427 (1954).
- [20] F. Kadijk and F. Jellinek, The system niobium-sulfur, *J. Less-Common Met.* **19**, 421 (1969).
- [21] G. F. Hardy and J. K. Hulm, The superconductivity of some transition metal compounds, *Phys. Rev.* **93**, 1004 (1954).
- [22] P. B. V. Narayan and D. K. Finnemore, Superconductivity in the niobium and scandium monosulfide systems at pressures up to 20 kbar, *J. Less-Common Met.* **61**, 231 (1978).
- [23] E. Amberger, K. Polborn, P. Grimm, M. Dietrich, and B. Obst, Superconductivity in the Nb cluster compounds Nb₃(X,Y)₄ with X, Y S, Se, Te, *Solid State Commun.* **26**, 943 (1978).
- [24] F. Jellinek, G. Brauer, and H. Müller, Molybdenum and niobium sulphides, *Nature (London)* **185**, 376 (1960).
- [25] J. Rijnsdorp and F. Jellinek, The crystal structure of niobium trisulfide, NbS₃, *J. Solid State Chem.* **25**, 325 (1978).
- [26] R. Lucrezi and C. Heil, Superconductivity and strong anharmonicity in novel Nb-S phases, *J. Phys.: Condens. Matter* **33**, 174001 (2021).
- [27] Y. An, J. Chen, Y. Yan, J. Wang, Y. Zhou, Z. Wang, C. Ma, T. Wang, R. Wu, and W. Liu, Higher-order topological and nodal superconducting transition-metal sulfides *MS* (*M* = Nb and Ta), *Phys. Rev. B* **108**, 054519 (2023).

- [28] A. Jain, S. P. Ong, G. Hautier *et al.*, Commentary: The materials project: A materials genome approach to accelerating materials innovation, *APL Mater.* **1**, 011002 (2013).
- [29] T. Zhang, Y. Jiang, Z. Song, H. Huang, Y. He, Z. Fang, H. Weng, and C. Fang, Catalogue of topological electronic materials, *Nature (London)* **566**, 475 (2019).
- [30] Y. Liang, M. Chen, Y. Wang, H. Jia, T. Lu, F. Xie, G. Cai, Z. Wang, S. Meng, and M. Liu, A universal model for accurately predicting the formation energy of inorganic compounds, *Sci. China Mater.* **66**, 343 (2023).
- [31] K. Onabe, M. Naito, and S. Tanaka, Anisotropy of upper critical field in superconducting $2H\text{-NbS}_2$, *J. Phys. Soc. Jpn.* **45**, 50 (1978).
- [32] B. Toby, Expgui, a graphical user interface for GsAs, *J. Appl. Crystallogr.* **34**, 210 (2001).
- [33] R. Prozorov and V. G. Kogan, Effective demagnetizing factors of diamagnetic samples of various shapes, *Phys. Rev. Appl.* **10**, 014030 (2018).
- [34] P. Giannozzi, S. Baroni, N. Bonini, M. Calandra, R. Car, C. Cavazzoni, D. Ceresoli, G. L. Chiarotti, M. Cococcioni, I. Dabo *et al.*, QUANTUM ESPRESSO: A modular and open-source software project for quantum simulations of materials, *J. Phys.: Condens. Matter* **21**, 395502 (2009).
- [35] D. R. Hamann, Optimized norm-conserving Vanderbilt pseudopotentials, *Phys. Rev. B* **88**, 085117 (2013).
- [36] H. Franzen, T. Beineke, and B. Conard, The crystal structure of Nb_{21}S_8 , *Acta Cryst. B* **24**, 412 (1968).
- [37] H. Chen, R. Tuenge, and H. Franzen, Preparation and crystal structure of Nb_{14}S_5 , *Inorg. Chem.* **12**, 552 (1973).
- [38] M. Tinkham, *Introduction to Superconductivity* (McGraw-Hill, New York, USA, 1996).
- [39] I. Guillamón, H. Suderow, S. Vieira, L. Cario, P. Diener, and P. Rodiere, Superconducting density of states and vortex cores of $2H\text{-NbSe}_2$, *Phys. Rev. Lett.* **101**, 166407 (2008).
- [40] P. Swartz and C. Bean, A model for magnetic instabilities in hard superconductors: The adiabatic critical state, *J. Appl. Phys.* **39**, 4991 (1968).
- [41] M. R. Wertheimer and J. le G. Gilchrist, Flux jumps in type II superconductors, *J. Phys. Chem. Solids* **28**, 2509 (1967).
- [42] C. Romero-Salazar, F. Morales, R. Escudero, A. Durán, and O. A. Hernández-Flores, Flux jumps in hot-isostatic-pressed bulk MgB_2 superconductors: Experiment and theory, *Phys. Rev. B* **76**, 104521 (2007).
- [43] A. Pramanik, S. Aswartham, A. Wolter, S. Wurmehl, V. Kataev, and B. Büchner, Flux dynamics and avalanches in the 122 pnictide superconductor $\text{Ba}_{0.65}\text{Na}_{0.35}\text{Fe}_2\text{As}_2$, *J. Phys.: Condens. Matter* **25**, 495701 (2013).
- [44] C.-R. Hu, Numerical constants for isolated vortices in superconductors, *Phys. Rev. B* **6**, 1756 (1972).
- [45] H. Padamsee, J. Neighbor, and C. Shiffman, Quasiparticle phenomenology for thermodynamics of strong-coupling superconductors, *J. Low Temp. Phys.* **12**, 387 (1973).
- [46] J. Bardeen, L. N. Cooper, and J. R. Schrieffer, Theory of superconductivity, *Phys. Rev.* **108**, 1175 (1957).
- [47] W. L. McMillan, Transition temperature of strong-coupled superconductors, *Phys. Rev.* **167**, 331 (1968).
- [48] Y. Hinuma, G. Pizzi, Y. Kumagai, F. Oba, and I. Tanaka, Band structure diagram paths based on crystallography, *Comput. Mater. Sci.* **128**, 140 (2017).
- [49] E. Revolinsky, G. Spiering, and D. Beerntsen, Superconductivity in the niobium-selenium system, *J. Phys. Chem. Solids* **26**, 1029 (1965).
- [50] H. Lian, Y. Wu, H. Xing, S. Wang, and Y. Liu, Effect of stoichiometry on the superconducting transition temperature in single crystalline $2H\text{-NbS}_2$, *Physica C* **538**, 27 (2017).
- [51] K. Momma and F. Izumi, *vesta 3* for three-dimensional visualization of crystal, volumetric and morphology data, *J. Appl. Crystallogr.* **44**, 1272 (2011).